Original Article

MOLECULAR METABOLISM

Maternal obesity alters fatty acid oxidation, AMPK activity, and associated DNA methylation in mesenchymal stem cells from human infants

Kristen E. Boyle [1,*], Zachary W. Patinkin [1], Allison L.B. Shapiro [2], Carly Bader [1], Lauren Vanderlinden [3], Katerina Kechris [3], Rachel C. Janssen [4], Rebecca J. Ford [5], Brennan K. Smith [5], Gregory R. Steinberg [5,6], Elizabeth J. Davidson [7], Ivana V. Yang [7], Dana Dabelea [3,8], Jacob E. Friedman [4]

ABSTRACT

Objective: Infants born to mothers with obesity have greater adiposity, ectopic fat storage, and are at increased risk for childhood obesity and metabolic disease compared with infants of normal weight mothers, though the cellular mechanisms mediating these effects are unclear.
Methods: We tested the hypothesis that human, umbilical cord-derived mesenchymal stem cells (MSCs) from infants born to obese (Ob-MSC) versus normal weight (NW-MSC) mothers demonstrate altered fatty acid metabolism consistent with adult obesity. In infant MSCs undergoing myogenesis *in vitro*, we measured cellular lipid metabolism and AMPK activity, AMPK activation in response to cellular nutrient stress, and MSC DNA methylation and mRNA content of genes related to oxidative metabolism.
Results: We found that Ob-MSCs exhibit greater lipid accumulation, lower fatty acid oxidation (FAO), and dysregulation of AMPK activity when undergoing myogenesis *in vitro*. Further experiments revealed a clear phenotype distinction within the Ob-MSC group where more severe MSC metabolic perturbation corresponded to greater neonatal adiposity and umbilical cord blood insulin levels. Targeted analysis of DNA methylation array revealed Ob-MSC hypermethylation in genes regulating FAO (*PRKAG2*, *ACC2*, *CPT1A*, *SDHC*) and corresponding lower mRNA content of these genes. Moreover, MSC methylation was positively correlated with infant adiposity.
Conclusions: These data suggest that greater infant adiposity is associated with suppressed AMPK activity and reduced lipid oxidation in MSCs from infants born to mothers with obesity and may be an important, early marker of underlying obesity risk.

Keywords Maternal/fetal; Obesity; AMPK; Lipid metabolism; Mesenchymal stem cells

1. INTRODUCTION

The developmental origins of health and disease hypothesis describes how intrauterine and early life stressors can alter the structure and function of fetal cells and tissues, thus changing offspring physiology and metabolism. Epidemiological data indicate that obesity during pregnancy is an important contributor to adiposity and metabolic disease risk in the offspring, independent of postnatal exposures [1,2]. Across multiple species, including humans, maternal obesity results in excess adiposity in fetal and/or adult offspring, both in adipose tissue depots and as ectopic fat stores in liver and skeletal muscle [3–8]. Such ectopic fat deposition in skeletal muscle is well-documented in adults with established obesity and linked to perturbations in fatty acid metabolism [9], but whether maternal obesity alters lipid partitioning in human offspring is not clear.

At the cellular level, animal models demonstrate that obesity during pregnancy accelerates fetal adipogenesis and alters lipid balance and energy metabolism, affecting both adipocytes and skeletal myocytes [7,10]. *In utero*, skeletal muscle and adipose tissues both develop from mesenchymal stem cells (MSC), which also reside in these developed tissues for repair and maintenance (e.g. adipose stromovascular [SV] cells, skeletal muscle satellite cells). Thus, perturbations to the MSC lineage not only may alter tissue development *in utero* but also may maintain altered tissue phenotype throughout life. For example, skeletal muscle satellite cells from adults with established obesity and/or type 2 diabetes exhibit altered lipid partitioning when differentiated to myotubes *in vitro*. These metabolic outcomes often track with the *in vivo* metabolic phenotype of the donor [9,11,12], suggesting that the origins of altered lipid partitioning may be genetic or epigenetic in origin. However, it is unclear if these differences were present prior to the development of obesity or diabetes.

[1]Section of Nutrition, Department of Pediatrics, University of Colorado School of Medicine, Aurora, CO, USA [2]Department of Epidemiology, Colorado School of Public Health, Aurora, CO, USA [3]Department of Biostatistics & Bioinformatics, Colorado School of Public Health, Aurora, CO, USA [4]Section of Neonatology, Department of Pediatrics, University of Colorado School of Medicine, Aurora, CO, USA [5]Department of Medicine, McMaster University, Hamilton, Ontario, Canada [6]Department of Biochemistry and Biomedical Sciences, McMaster University, Hamilton, Ontario, Canada [7]Department of Medicine, University of Colorado School of Medicine, Aurora, CO, USA [8]Department of Pediatrics, University of Colorado School of Medicine, and the Lifecourse Epidemiology of Adiposity and Diabetes (LEAD) Center, Aurora, CO, USA

*Corresponding author. Department of Pediatrics, University of Colorado Anschutz Medical Campus, MS C225, 12700 E. 19th Ave, Aurora, CO, 80045, USA. Fax: +1 303 724 6636. E-mail: kristen.boyle@ucdenver.edu (K.E. Boyle).

Received July 14, 2017 • Revision received August 22, 2017 • Accepted August 25, 2017 • Available online 1 September 2017

http://dx.doi.org/10.1016/j.molmet.2017.08.012

Abbreviations

ACC	acetyl CoA carboxylase
ACL	ATP citrate lyase
AICAR	5-aminoimidazole-4-carboxamide ribonucleotide
AMPK	AMP-activated protein kinase
ASM	acid soluble metabolite
CPT	carnitine palmitoyl transferase
DGAT1	diacylglycerol acyltransferase
DMR	differentially methylated region
ETS	electron transport system
EWAS	epigenome-wide association studies
FAO	fatty acid oxidation
FAS	fatty acid synthase
FFA	free fatty acid
FM	fat mass
GM	growth medium (undifferentiated MSCs)
HOMA-IR	homeostatic model assessment-insulin resistance
SDH	succinate dehydrogenase
MIM	myogenic induction medium (myogenic differentiating MSCs)
MSC	mesenchymal stem cell
NW	normal weight
Ob	obese
ORO	Oil Red O
PPAR	peroxisome proliferator activated receptor
Raptor	regulatory associated protein of MTOR complex 1
SCD1	stearoyl-CoA desaturase 1
SNP	single nucleotide polymorphism
SREBP1	sterol regulatory element-binding protein 1
SV	stromovascular
TCA	tricarboxylic acid
TSS	transcription start site

Intrauterine development is a period of rapid growth and epigenetic remodeling, during which the fetus is particularly vulnerable to conditions that may adversely impact tissue development and disease propensity later in life. Epigenetic modifications observed in fetal tissues and tissue-derived MSCs from animals exposed to intrauterine obesity [13–15] suggest that cell-autonomous MSC predisposition may be present from birth. For example, SV cells from offspring of obese rodents exhibit greater adipogenesis when induced *in vitro* [13,14]. In primates, oxidative metabolism is reduced not only in fetal skeletal muscle from obese dams but also in fetal muscle-derived satellite cells when differentiated to myotubes *in vitro* [10]. Together, these findings suggest that altered metabolism occurs during fetal development in the offspring MSC, prior to the onset of overt obesity. One notable early example of human epigenetic modification is hypermethylation of the *RXRA* gene promoter in umbilical cord tissue that was associated with greater adiposity at age nine [16]. These findings suggest that genes regulating lipid metabolism may be altered in human neonatal tissues and predict risk for greater adiposity later in life. To date, a major limitation of such epigenetic studies in human infants is a lack of specificity for cell population or direct measures of corresponding mRNA content, protein content, or pathway function. However, umbilical cord tissue is a robust source of fetal MSCs that can be differentiated *in vitro* into biologically relevant cell types as a model for investigating the functional implications of adverse intrauterine exposures. We have reported that human umbilical cord-derived MSCs from infants born to mothers with obesity exhibit greater adipogenesis *in vitro* [4]. Moreover, we found that lipid content of the adipogenic differentiating MSCs correlated with neonatal adiposity [4]. Here, we investigated cellular lipid metabolism and AMPK activity in infant MSCs undergoing myogenesis *in vitro*. We hypothesized that MSCs from infants of obese mothers would demonstrate altered lipid partitioning and lower fatty acid oxidation, as observed in adults with established obesity and in MSCs from animal models of maternal obesity. We also investigated the regulation of AMPK in response to cellular nutrient stress and potential epigenetic mechanisms for our observed metabolic differences.

2. MATERIALS AND METHODS

2.1. Ethics statement

This study used umbilical cord tissue samples and other data collected by the Healthy Start Study (ClinicalTrials.gov; NCT02273297). Approval for this study was obtained from the Colorado Multiple Institutional Review Board at the University of Colorado Hospital. Written, informed consent was obtained from all participants at enrollment.

2.2. Subjects

The Healthy Start longitudinal pre-birth cohort study enrolled 1410 pregnant women ages 16 and older, $\leq$23 weeks gestation, recruited from the obstetrics clinics at the University of Colorado Hospital during 2010–2014. Women were excluded if they had prior diabetes, prior premature birth, serious psychiatric illness, or a current multiple pregnancy. MSCs from 165 infants were collected under the mechanistic arm of Healthy Start: BabyBUMP, from which 15 normal-weight and 14 obese mothers were selected, as described in detail [4]. Data collection for Healthy Start has been previously described [5]. Briefly, pregnant women were evaluated at median weeks 17 and 27 gestation for demographics, tobacco use, height, and weight. Fasting blood samples were drawn for measures of glucose, insulin, triglycerides, and free fatty acids (FFA). Pre-pregnancy BMI was obtained through medical record abstraction (84%) or self-report at the first research visit (16%). Gestational weight gain was defined as the difference between pre-pregnancy weight and weight at delivery. Infant birth weight was obtained from medical records and infant weight, length, and body composition (fat mass [FM], fat-free mass [FFM]; whole body air plethysmography [PEA POD, COSMED, Inc.]) were measured within 24–48 h after birth.

2.3. MSC isolation and culture

MSCs were cultured from fresh umbilical cord tissue explants of normal-weight (NW-MSC; n = 15) and obese (Ob-MSC; n = 14) mothers, as described [4]. As previously described, MSCs were >98% positive for MSC markers CD73, CD90, and CD105, and were negative for hematopoietic and lymphocyte markers CD34, CD45, and CD19 [4]. All experiments were performed on cells in passages 4–6. Myogenesis was induced for 21 d, as described [4,17]. In our hands, MSCs express appropriate adipogenic or skeletal myogenic markers with respective induction *in vitro* [4]. Our previous report showed no difference in myogenic markers between NW- and Ob-MSCs, with similar percentages of cells expressing myogenin protein, as measured by flow cytometry [4]. Measures were made in MSCs with growth medium only (GM, undifferentiated) or following 21d of myogenic induction medium (MIM, myogenic differentiating), as indicated.

2.4. Lipid accumulation and ^{14}C lipid metabolism assays

Following 21 d of myogenesis, cells were fixed with 4% formaldehyde and stained for ORO neutral lipid content, as described [4]. ^{14}C-labeled fatty acid oxidation (FAO) was measured using 200 μM oleate and palmitate (2:1 ratio) with 1 mM carnitine, as described [18]. This method measures both complete oxidation of fatty acids to CO_2 and incomplete oxidation of fatty acids as determined by acid soluble metabolites (ASM)s. FAO is the sum of these component measures. For lipid esterification and total lipid uptake assays, ^{14}C-esterified lipids were extracted by chloroform/methanol and total content of ^{14}C was measured in cell lysates. Total cellular lipid uptake is calculated as the total FAO + cell lysate measures. All measures were performed in triplicate, and data were corrected for total protein content, as measured by BCA method (bicinchoninic acid assay; Pierce Biotechnology, Inc.).

2.5. Glycolysis and glucose uptake assays

Following 21 d of myogenic induction, media was freshly replaced with either media alone or media supplemented with 100 mM 2-deoxyglucose or 1 μg/mL oligomycin. Cells were incubated 2 h at 37 °C and L-lactate accumulation was measured in the media using the Glycolysis Cell-Based Assay Kit (Cayman Chemical, Ann Arbor, MI). Data were corrected for values in a no cell control well and for total protein content, as measured by BCA method. ^{3}H-2 deoxyglucose uptake was measured as described [19] in 21 d myogenic differentiating cells as an index of basal glucose uptake. Data were normalized to wells treated with cytochalasin B as a negative control and to total protein content.

2.6. Enzyme activity assays

Pelleted cells were flash frozen for later preparation of mitochondrial-enriched supernatants and measures of citrate synthase (CS) activity in duplicate, as previously described [20]. Total carnitine palmitoyl transferase (CPT) activity was measured as described with minor modification [21]. Briefly, mitochondria were freshly isolated by differential centrifugation [21]. Total CPT activity was measured in quadruplicate spectrophotometrically. Protein content was determined by BCA assay and used to normalize enzyme activity measures.

2.7. Protein measures

Cells were harvested in lysis buffer (CelLytic™ MT, Sigma—Aldrich, St. Louis, MO) supplemented with protease and phosphatase inhibitor cocktails (Sigma—Aldrich). Total protein was determined by BCA assay. Protein content of diacylglycerol acyltransferase (DGAT)1, sterol regulatory element binding protein (SREBP)1, fatty acid synthase (FAS), stearoyl-CoA desaturase (SCD)1, ATP citrate lyase (ACL) ^{S455}/ACL, AMPKα ^{Thr172}/AMPKα, and acetyl CoA carboxylase (ACC) $^{Ser79/212}$/ACC, with β-actin as reference control by Simple Western size-based protein assay (WES, ProteinSimple, Santa Clara, CA) following manufacturer's protocol. Results from WES were analyzed using ProteinSimple Compass software. All antibodies were optimized in-house for this system and antibody specifics and assay conditions are listed in Supplemental Table 1. Western blotting for AMPKα ^{Thr172}/AMPKα, ACC $^{Ser79/212}$/ACC, regulatory associated protein of MTOR complex 1 (raptor) ^{Ser792}/raptor, or Mitoprofile OXPHOS antibody cocktail, which measures electron transport system (ETS) complexes, were performed as described [22]. Antibodies and conditions are detailed in Supplemental Table 1.

2.8. RNA isolation and qPCR

Cells were harvested in Buffer RLT Plus (Qiagen). Total RNA was isolated using RNeasy Plus mini kit (Qiagen) and cDNA transcribed from 1 μg total RNA using iScript cDNA Synthesis kit (Bio-Rad, Hercules, CA). qPCR was performed using Taqman Gene Expression Assays with Taqman Fast Advanced Mastermix (Thermo Fisher Scientific, Waltham, MA) for genes of interest with *ACTB* and *GAPDH* as reference genes with a no-template control per gene. Reactions were run in triplicate on a Viia 7 Real Time PCR System (Thermo Fisher). Data were normalized using the geometric mean of the reference genes. Gene IDs and primer information are listed in Supplemental Table 2.

2.9. DNA isolation and 450 K methylation array

Genomic DNA was purified from undifferentiated MSCs with proteinase K digestion and extraction using the QIAamp DNA mini kit (Qiagen, Germantown, MD), according to manufacturer's protocol. Total double-stranded DNA was measured using Qubit™ (Thermo Fisher Scientific). DNA (1 μg) was bisulfite-converted using the EZ DNA Methylation kit (Zymo Research, Irvine, CA), according to manufacturer's protocol. Illumina's Infinium Human Methylation 450 K BeadChip (Illumina, San Diego, CA) was used to measure DNA methylation on bisulfite-treated genomic DNA from undifferentiated MSCs at the Genomics and Microarray Core at University of Colorado Anschutz Medical Campus. All samples were assayed in one batch.

2.10. CpG bisulfite pyrosequencing

For the genesets analyzed, we selected three CpGs, one from each of the differentially methylated regions identified (cg02022322, cg17058475, cg20534694) as significantly different to independently verify the CpG sites identified in this study by bisulfite pyrosequencing. Bisulfite-converted DNA was PCR amplified using primers designed in the Pyromark Assay Design Software (Qiagen, Germantown, MD). Pyrosequencing was performed on the PyroMark Q96 MD sequencer (Qiagen, Germantown, MD) using reagents and protocols supplied by the manufacturer. PCR and sequencing were performed in triplicate for each sample. Each plate contained 0%, 50%, and 100% methylated controls. Percent methylation was calculated from the peak heights of C and T using the Pyro Q-CpG software (Qiagen, Germantown, MD). We were unable to adequately optimize one set of primers (cg20534694); therefore, we only reported the remaining two.

2.11. Statistical analyses for individual MSC data

D'Agostino & Pearson tests were used to assess normality of the data. Levene's tests were used to assess unequal variance. For testing comparisons between groups, independent *t*-tests or Mann—Whitney U tests were used, where appropriate. For comparison of three groups (NW-MSC, ObLo-MSC, ObHi-MSC) data were analyzed using analysis of variance (ANOVA) with planned contrasts to evaluate the data as three independent groups, as well as NW- versus Ob-MSC differences. For treatment experiments, paired *t*-tests were used for comparison of control versus treatment conditions for all MSCs combined. Pearson correlations were used to identify relationships between MSC methylation and maternal and infant measures, with Bonferroni correction for multiple testing. All data are expressed as mean ± SEM. Differences between groups were considered statistically significant if $P \leq 0.05$.

2.12. Statistical analyses for methylation array

All arrays passed a sample-specific quality control where the log2 transformed intensities for both the methylated and unmethylated channels were examined for having sufficient intensity levels. Individual probes that failed in 10% of samples (based on detection P-values) or had a low bead count (<3 beads) were removed from the analysis. The remaining probes were mapped to the human genome

(GRCh37/hg19). Probes that did not uniquely align to the genome were removed. Probes containing a known single-nucleotide polymorphism (SNP) were kept in the analysis, but flagged. Arrays were then normalized using subset-quantile within array normalization (SWAN). Both M values (log2 of methylated to unmethylated ratio) and β-values (proportion of sites methylated) were produced. The normalized M values were used for all subsequent analyses, whereas the β-values on the scale of 0%—100% are reported to facilitate biological interpretation. Array processing and quality control was performed in R (v. 3.2.0) using the minfi (v.1.14.0) [23] and wateRmelon (v.1.8.0) [24] packages.

Only sites located within selected genes specific to oxidative metabolism were included for statistical analyses (68 genes, 1,174 CpG sites; Supplemental Tables 3 and 4), with multiple testing adjusted for the number of CpGs included in the analysis. A kernel smoothing method for differentially methylated region (DMR) analysis using the DRMcate package in R (v.1.4.2) [25], was performed to identify DMRs between NW- and Ob-MSCs, while adjusting for gestational weight gain and infant sex. DMRs with $P < 0.05$ were considered significant. The number of probes included in these regions, genomic coordinates, mean β-values for each probe in the DMR, and the minimum P-value adjusted for multiple testing, across the region are reported (Supplemental Table 5). Mean β-values for each probe analyzed are reported in Supplemental Table 6.

3. RESULTS

3.1. Maternal and infant characteristics

By design, mothers with obesity had higher BMI, but similar maternal age, gestational age at delivery, infant sex, and time to confluence for initial MSC culture (Table 1). Mothers with obesity had greater insulin resistance (homeostatic model assessment for insulin resistance [HOMA-IR]) and elevated fasting insulin and FFA levels, though none had pre-existing diabetes or previous gestational diabetes, and none developed gestational diabetes during the index pregnancy. The infants of the obese mothers had similar birth weight, higher cord blood insulin levels, and higher percentage fat mass measured 24—48 h after birth.

Table 1 — Maternal and infant characteristics.

	NW (n = 15)	Obese (n = 14)	P
Maternal characteristics			
Age (y)	28.0 ± 1.5	26.7 ± 1.9	0.60
Pre-pregnancy BMI (kg/m^2)	21.1 ± 0.3	34.6 ± 1.0	<0.001*
Primiparous, n (%)	6 (40.0)	6 (42.9)	0.88
Glucose (mmol/L)	4.1 ± 0.1	4.2 ± 0.1	0.39
Insulin (pmol/L)	53.2 ± 3.6	87.1 ± 11.6	0.01*
HOMA-IR	2.1 ± 0.3	3.1 ± 0.4	0.08
Triglycerides (mmol/L)	1.5 ± 0.2	1.6 ± 0.1	0.64
Free fatty acids (mmol/L)	334.9 ± 28.0	471.8 ± 44.2	<0.01*
Gestational weight gain (kg)	14.2 ± 0.9	10.2 ± 2.2	0.08
Gestational age at delivery (wk)	39.9 ± 0.2	39.7 ± 0.3	0.52
Cesarean delivery, n (%)	2 (13.3)	2 (14.3)	0.94
Infant characteristics			
Sex, n (f/m)	8/7	9/5	0.57
Birth weight (g)	3316.8 ± 94.7	3325.9 ± 102.5	0.95
Birth length (cm)	49.8 ± 0.5	49.3 ± 0.5	0.49
Fat mass (g)	270.0 ± 31.8	358.3 ± 34.7	0.07
Fat mass (%)	8.43 ± 0.9	11.1 ± 0.9	0.05*
Fat free mass (g)	2877.8 ± 62.3	2836.3 ± 92.8	0.71
Fat free mass (%)	91.6 ± 0.9	88.9 ± 0.9	0.05*
Cord blood glucose (mmol/L)	4.2 ± 0.3	4.0 ± 0.2	0.79
Cord blood insulin (pmol/L)	40.4 ± 5.3	68.1 ± 10.9	0.03*
MSC characteristics			
Culture time to confluence (d)	26.3 ± 1.2	26.7 ± 1.9	0.84

Data are mean ± SEM, unless otherwise stated. * Significant independent *t*-test $P \leq 0.05$.

3.2. Greater lipid content and lower FAO in Ob-MSCs

To determine cellular neutral lipid content in 21d myogenic differentiating MSCs, we stained cells with Oil Red-O (ORO) and observed 30% higher staining in Ob-versus NW-MSCs (Figure 1A). ORO was localized as droplets within the cell and not accompanied by elevated content of the adipogenic marker peroxisome proliferator activated receptor (PPAR)γ (Supplemental Figure 1a), suggesting that there was not spontaneous adipogenesis in the Ob-MSCs. Greater lipid storage in Ob-MSCs could be due to upregulation of lipogenic pathways, though we observed no differences between NW- and Ob-MSCs for the triglyceride synthesis regulator DGAT1 (Figure 1B) or for proteins regulating *de novo* lipogenesis: ACL, ACC, SREBP1, FAS, SCD1 (Supplemental Figure 1b—d). To determine cellular lipid uptake and metabolism, we performed radiolabeled lipid tracer experiments in myogenic differentiating MSCs using a physiological composition of ^{14}C-labeled fatty acids plus carnitine, which is less cytotoxic than palmitate [26]. We observed no difference in total cellular uptake of fatty acids, though esterified lipids were 30% higher and total ^{14}C-FAO was 30% lower in the Ob-versus NW-MSCs (Figure 1C). Lower FAO could be due to increased availability of glycolytic products (i.e. greater reliance on carbohydrate substrate), though we did not observe group differences in glycolysis with MIM alone or minimal or maximal glycolytic rates (2-deoxyglucose or oligomycin, respectively; Figure 1D). Likewise, we did not observe differences in basal cellular glucose uptake (Supplemental Figure 1e). Together, these data indicate that, of a comparable amount of fatty acids entering the cell during the measurement period, fewer are oxidized and more are stored in Ob-MSCs. These differences in lipid metabolism are not attributable to differences in lipid or carbohydrate uptake.

3.3. Distinct metabolic phenotypes identified among Ob-MSCs

Total FAO (Figure 1C) is the sum of two component measures: complete oxidation of fatty acids to CO_2 and incomplete oxidation (ASMs), which represents fatty acids that entered the mitochondria but were not completely metabolized. The ratio of ASM/CO_2 represents mitochondrial efficiency for fatty acid oxidation, where higher values reflect deficits within the mitochondria, either in β-oxidation or the tricarboxylic acid (TCA) cycle. Importantly, ASM/CO_2 is typically elevated in skeletal muscle tissue and cells from obese animals and humans [26—29] and mitochondrial inefficiency for fat oxidation has been causally linked to the development of insulin resistance in animal models [26]. When we closely examined ASM/CO_2, we discovered a clear divergence among the Ob-MSCs that tracked with differences in complete oxidation (CO_2), but not with ASM (Figure 2A—C). Importantly, there was no divergence among the Ob-MSCs for ORO, total FAO, fatty acid uptake, or esterification (*data not shown*). These results indicate that, while all Ob-MSCs have greater lipid accumulation and deficits in total mitochondrial uptake of fatty acids (FAO), a subset of Ob-MSCs have lower complete oxidation (CO_2), which could have important implications for mitochondrial health. In fact, animal models of maternal obesity show disruption to multiple aspects of mitochondrial health in the offspring [10,30].

We hypothesized that the distinct Ob-MSC phenotypes we observed may be reflective of distinct intrauterine exposures associated with maternal obesity. Thus, we separated the Ob-MSC into ObLo and ObHi according to ASM/CO_2 (Figure 2A) and re-evaluated maternal and

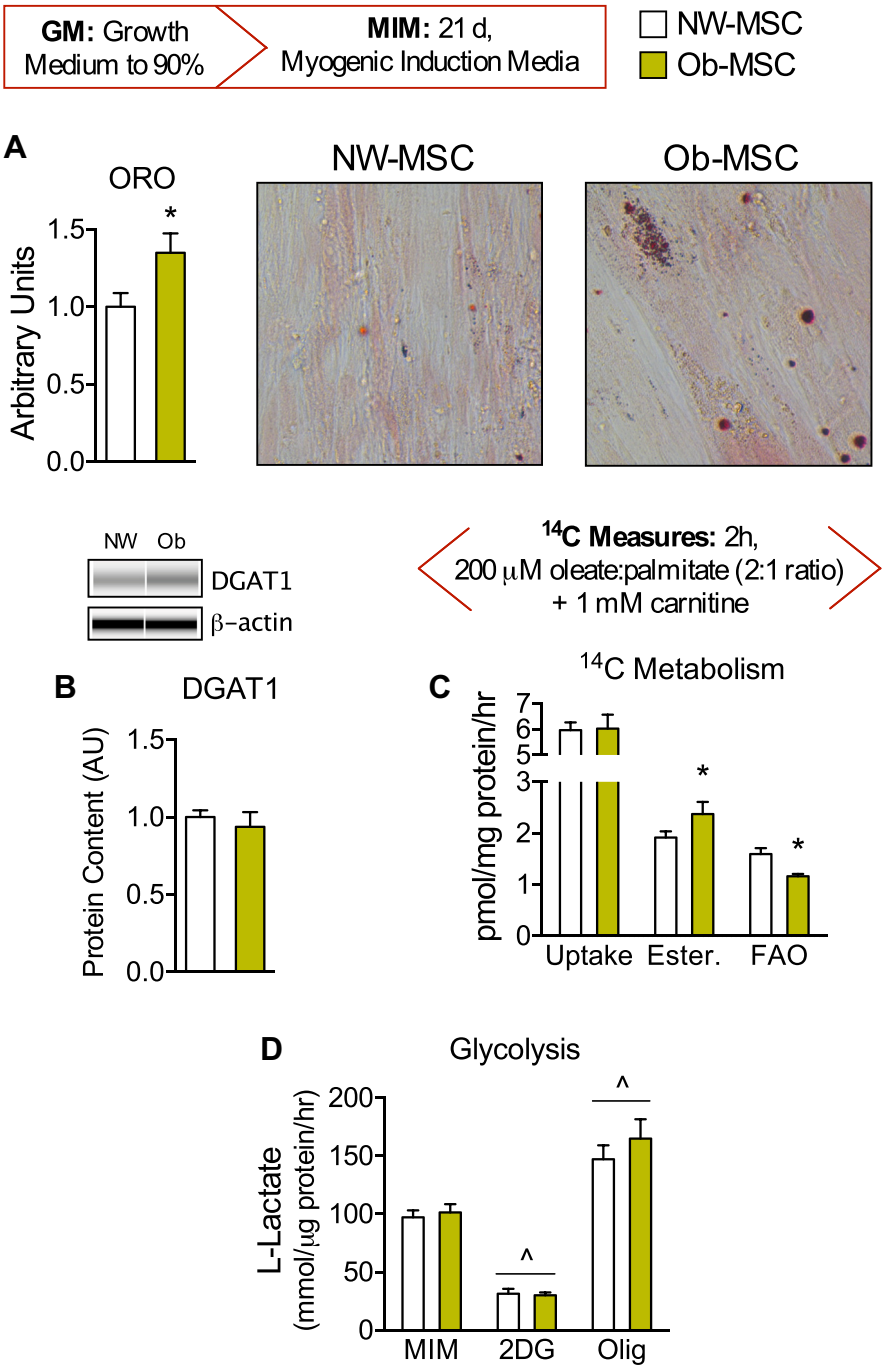

Figure 1: Greater lipid content and lower FAO in Ob-MSCs, see also Supplemental Figure 1. Cells were grown to 90% confluence in growth medium (GM) and underwent myogenic induction (MIM) for 21 days. (**A**) ORO staining was quantified spectrophotometrically at day 21 of myogenesis in NW- and Ob-MSCs, with representative light microscope images taken at 20× magnification. Data are presented in arbitrary units as the fold-difference in Ob-MSCs relative to NW-MSCs with mean ± SEM (5 technical replicates per subject). (**B**) Simple Western measures of DGAT1 protein content was measured cells following 21 days of MIM. β-actin serves as a loading control. Data are presented in arbitrary units as the fold-difference in Ob-MSCs relative to NW-MSCs with mean ± SEM (2 culture replicates per subject, pooled). (**C**) At d21 of myogenesis, fatty acid tracer measurements were made using ^{14}C[oleate:palmitate] in conditions depicted. Total cellular ^{14}C lipid uptake, total ^{14}C esterified lipids, and total ^{14}C FAO were measured. All ^{14}C data are presented as mean ± SEM for NW and Ob-MSC (3 technical replicates per subject). (**D**) Rates of glycolysis were determined for basal (untreated), minimal (2DG, 100 mM 2-deoxyglucose), and maximal (Olig, 1 μg/mL oligomycin) conditions by measuring accumulation of L-lactate in the culture media following 2 h of incubation. Data are presented as mean ± SEM for NW and Ob-MSC (2 technical replicates per subject). *P $<$ 0.05 for difference in NW- vs. Ob-MSC by 2-tailed Student's *t*-test or Mann–Whitney U Test, where appropriate. For all measures n $\geq$ 12 subjects/group. ^P $<$ 0.05 for difference from untreated condition for both NW- and Ob-MSC groups, combined using 2-way ANOVA. GM, growth Medium; MIM, myogenic induction medium; d, days; ORO, Oil Red O.

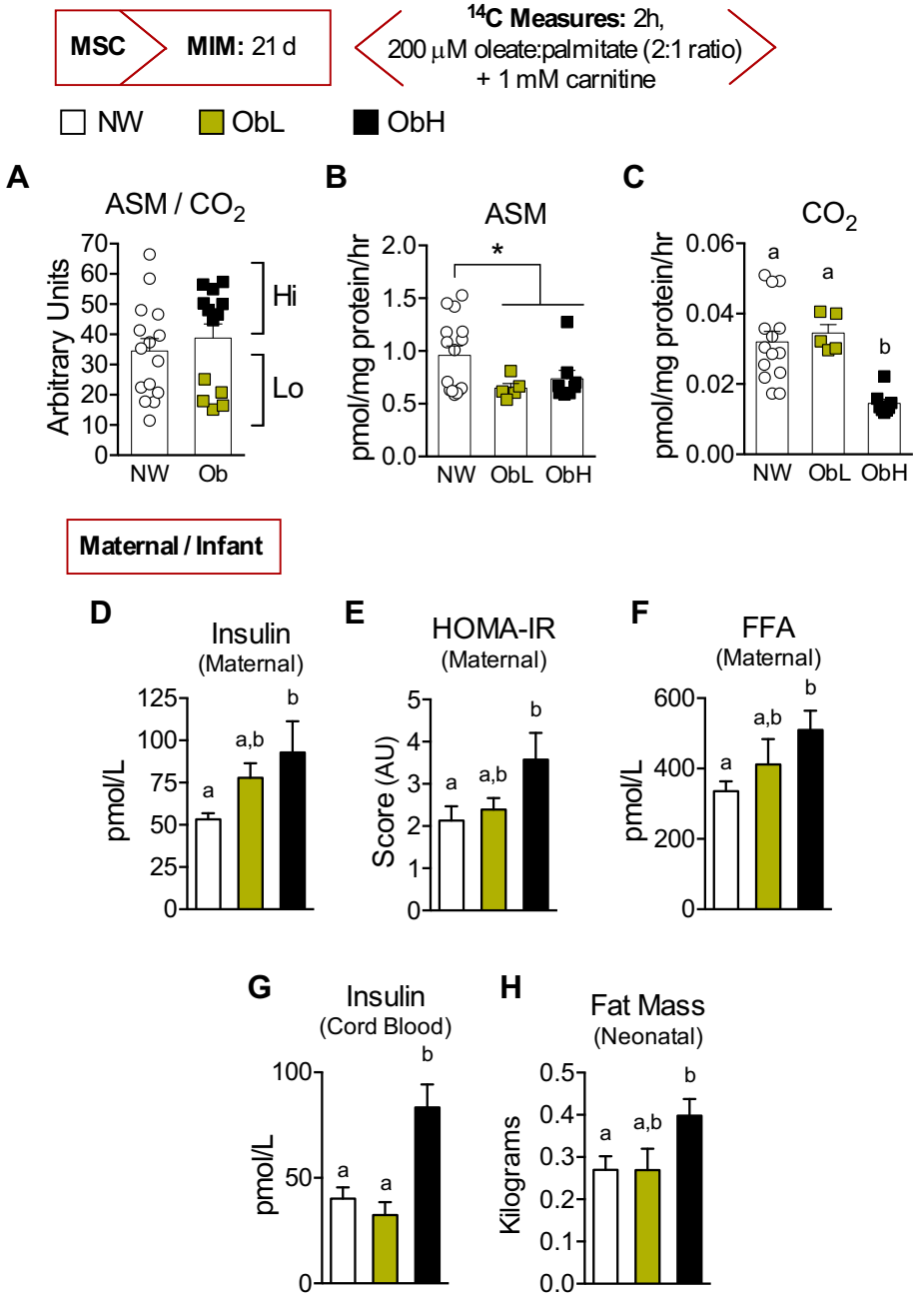

Figure 2: Distinct metabolic phenotypes identified among NW- and Ob-MSCs, see also Supplemental Figure 2. At d21 of myogenesis, FAO measurements were made using ^{14}C-[oleate:palmitate] in conditions depicted. (**A**) The ratio of incomplete FAO (ASM) and complete FAO to CO_2 (CO_2), reveals two distinct groups of Ob- and NW-MSCs which were further examined as separate groups to gain insight into the metabolic functioning of these cells. Frequency distributions of these data are shown in Supplemental Figure 2. (**B**) Incomplete FAO as determined by acid soluble metabolites (ASM). (**C**) Complete FAO to CO_2. (**D**—**F**) Maternal fasting insulin, HOMA-IR, and FFA levels were measured after overnight fast at median 17 weeks gestation. (**G**) Insulin was measured in cord blood collected immediately after birth. (**H**) Infant fat mass was measured using air displacement plethysmography within 24—48 h after birth. All data are presented as mean ± SEM. For each panel, bars with different letters indicate differences for those groups at $P < 0.05$ as calculated by ANOVA analysis with *a priori* planned comparisons for three independent groups, and comparison of NW-MSC versus all Ob-MSCs. MIM: myogenic induction media; FAO, fatty acid oxidation; ASM, acid soluble metabolite; HOMA-IR, homeostatic model assessment for insulin resistance; FFA, free fatty acids.

infant *in vivo* measures. We found no significant group differences between the Ob groups based on maternal BMI, infant sex, gestational age at delivery, gestational weight gain, birth weight, or maternal glucose levels (*data not shown*). Notably, however, maternal fasting insulin, HOMA-IR score, and FFA levels showed a stepped increase from NW < ObLo < ObHi (Figure 2D—F). Moreover, infant adiposity showed similar patterns for increasing severity and cord blood insulin levels were markedly higher in ObHi, with no difference in cord blood FFA levels (Figure 2G—H). Correlation analyses confirmed the stepped increases for these maternal and infant characteristics between groups (Supplemental Figure 2a—e). We interpret this to mean that intrauterine exposures contributing to differences in neonatal adiposity and cord blood insulin levels may also contribute to MSC phenotype differences.

To statistically evaluate these separate phenotypes we examined frequency distributions of NW- and Ob-MSCs and found that, while NW-MSCs displayed a relatively normal distribution for ASM/CO_2, the Ob-MSCs displayed a clear bimodal distribution, representative of distinct phenotypes (Supplemental Figure 2f–g). Moreover, separate examination of the NW-MSC group, similarly split at the mean for ASM/CO_2, does not reveal differences for any maternal or neonatal measures, nor for other MSC measures, such as CO_2. (*not shown*). Thus, we continued by evaluating the three groups separately, but also accounting for the Ob-MSC groups combined to identify measures consistent with maternal obesity alone (such as ORO, FAO), and those tracking with Ob-MSC phenotypes (such as CO_2).

3.4. Ob-MSCs demonstrate lower AMPK protein content

To examine the mechanisms contributing to lower total FAO observed in both Ob-MSC groups, we measured markers of mitochondrial content and observed no significant differences in citrate synthase enzyme activity or protein content of ETS complexes I–IV (Figure 3A–B). We next measured CPT enzyme activity in mitochondrial lysates and found that it was higher in all Ob-MSCs compared with NW-MSC (Figure 3C) indicating that, outside of the cellular environment, CPT capacity to activate fatty acids was not compromised in Ob-MSCs. In fact, higher CPT activity in Ob-MSCs may reflect compensation for deficits upstream of CPT.

Mitochondrial entry of fatty acids and, thus, FAO is acutely increased by AMPKα phosphorylation and inhibition of ACC, which relieves inhibition on CPT leading to increases in flux of fatty acyl-CoA into the mitochondria for oxidation [31]. We found that phosphorylated AMPK tended to be lower while total AMPKα1/2 was significantly lower in Ob- versus NW-MSCs (Figure 3D). These data suggest that reductions in AMPK content may be important for reducing FAO in all Ob-MSCs.

3.5. Lower AMPK activation in ObHi-MSCs

To further investigate differences in AMPK function/activation, we primed cells with excess fatty acids (24hFA) to increase lipid availability and activate AMPK. 24hFA ameliorated differences in total AMPK

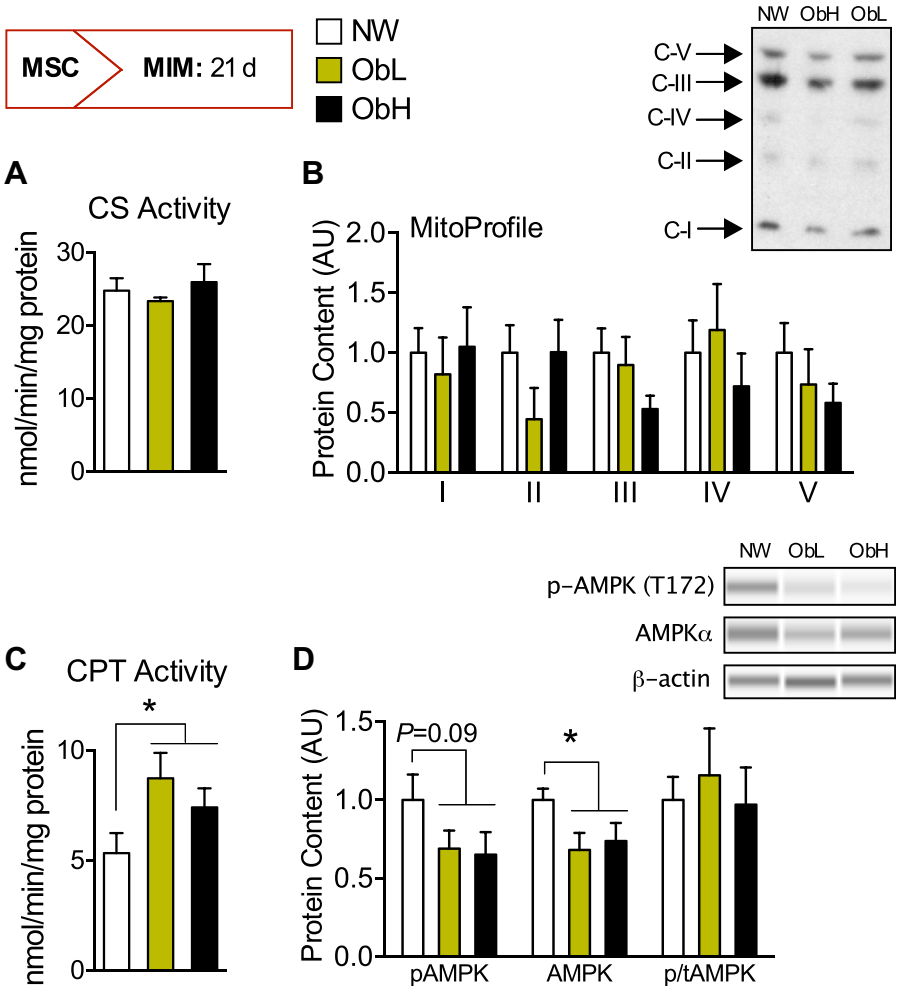

Figure 3: Ob-MSCs demonstrate lower AMPK protein content. (**A**) Citrate synthase (CS) activity was determined spectrophotometrically in cell lysates (2 technical replicates per subject). (**B**) Western blot analysis of ETS complex proteins (complexes I–V) was measured using the MitoProfile Antibody cocktail. Data are presented in arbitrary units as the fold-difference in Ob-MSCs relative to NW-MSCs with mean ± SEM (2 culture replicates per subject, pooled; n ≥ 5 subjects/group). (**C**) Total CPT activity was measured spectrophotometrically in isolated mitochondria (4 technical replicates per subject; n ≥ 3 subjects/group). (**D**) Simple Western measures of phosphorylated (Thr172) and total protein content of AMPKα1/α2 were measured. β-actin serves as a loading control. Data are presented in arbitrary units as the fold-difference relative to NW-MSCs (2 culture replicates per subject, pooled; n ≥ 5 subjects/group). All data are presented as mean ± SEM. For each panel, bars with different letters indicate differences for those groups at $P < 0.05$ as calculated by ANOVA analysis with *a priori* planned comparisons for three independent groups and comparison of NW-MSC versus all Ob-MSCs. MIM: myogenic induction media; CS, citrate synthase; CPT, carnitine palmitoyltransferase; AMPK, AMP-activated protein kinase.

and increased AMPK ^{Thr172}/AMPK protein in all groups, though to a lesser extent in ObHi (Figure 4A, Supplemental Figure 3a–b). As an index of AMPK activity, phosphorylated ACC increased with 24hFA in all cells (Supplemental Figure 3c–d), with greater ACC $^{Ser79/212}$/ACC content with 24hFA in ObLo (Figure 4B).

To more clearly define AMPK activation in the MSCs, independent of changes in fatty acid availability (i.e. 24hFA), we directly activated AMPK with 5-aminoimidazole-4-carboxamide ribonucleotide (AICAR; 24hAICAR), a pharmacological activator of AMPK that mimics cellular AMP. 24hAICAR increased AMPK ^{Thr172}/AMPK to a similar extent in all groups, ameliorating ObHi deficits in AMPK ^{Thr172}/AMPK observed with 24hFA (Figure 4C). 24hAICAR increased ACC $^{Ser79/212}$/ACC in all groups though, as with 24hFA, more robustly in ObLo (Figure 4D). There were no differences in total protein levels between groups or with treatment (Supplemental Figure 3e–h). We posited that consistently lower ACC $^{Ser79/212}$/ACC in NW-MSCs for 24hFA and 24hAICAR were related to differences in substrate preference rather than an inherent deficit in AMPK activity. To address this, we measured raptor^{Ser792}, another AMPK substrate. 24hAICAR robustly increased raptor^{Ser792}/raptor in NW and ObLo but not in ObHi (Figure 4E; Supplemental Figure 3i–j). These data indicate that, despite rescue of deficits in AMPK ^{Thr172}/AMPK with 24hAICAR, ObHi maintain deficits in AMPK activity, regardless of substrate. NW-MSC preference for raptor over ACC may be reflective of differences in cellular lipid content (Figure 1A), where NW-MSCs maintain greater capacity to store excess fuels and, thus, have less need for robust activation of FAO when under metabolic stress. Collectively, these data indicate that reductions in AMPK activity contribute to a reduced ability to regulate FAO and, while ObLo-MSCs respond robustly to nutrient stress and direct AMPK activation, ObHi-MSCs do not.

3.6. Ob-MSCs demonstrate hypermethylation of genes specific to FAO

We next investigated epigenetic differences linked to our metabolic observations using a hypothesis-driven approach (Figure 5A). We selected curated genesets specific to oxidative metabolism and the regulation of FAO (MSigDB, Broad Institute; Supplemental Tables 3 and 4). We then analyzed MSC Illumina 450 K methylation array data for DMRs in these genes. Because differences in methylation of specific loci can be small yet persistent across a DNA region, the DMR analysis is considered more informative than single CpG significance, combining information from multiple CpGs to improve the biological inference of the data [25]. We then confirmed DMR results by bisulfite pyrosequencing of select CpGs and measuring mRNA content.

Methylation analysis revealed hypermethylation in Ob-MSCs for *PRKAG2*, *ACACB*, *CPT1A*, and *SDHC* (maximum β-value differences in each DMR reflect 9%, 9%, 12% and 8% greater methylation in Ob- versus NW-MSC, respectively; Figure 5B–E, Supplemental Table 5). Mean β-values for all probes tested are reported in Supplemental Table 6. *PRKAG2*, *ACACB*, and *CPT1A* encode for subunits/isoforms of proteins regulating fatty acid mitochondrial entry (AMPKγ2, ACC2, CPT1A), while *SDHC* encodes for a subunit of ETS complex II (Figure 5F). All DMRs flank active transcription start sites (TSS; <1,500 bases) and/or are at known enhancer regions [32,33] (Figure 5B–E, Supplemental Figure 4). Only one common SNP was within 10 bases of the single base extension of any identified CpG site (*SDHC*:cg13788685; rs114165436). Pyrosequencing confirmed two CpG sites with the greatest Ob-MSC hypermethylation: *CPT1A*:cg17058475 and *ACACB*:cg02022322 (Figure 6A–B). qPCR revealed significantly lower or a trend for lower mRNA content for all genes in Ob- versus NW-MSCs, also measured in undifferentiated MSCs (GM, Figure 6C).

Our MSC lipid metabolism results are in line with reduced *PRKAG2* content and the known function of AMPKγ2, where ADP is more protective against AMPKα de-phosphorylation when the AMPK complex contains AMPKγ2 as opposed to AMPKγ1 or γ3 isoforms [34]. Moreover, AMP does not have a similar preference for AMPKγ2 where, in the presence of AMP, AMPKα phosphorylation is similar regardless of AMPKγ isoform [34]. This may explain why ObHi increased AMPK ^{Thr172}/AMPK to a similar extent as other groups with 24hAICAR, but not with 24hFA. Thus, we evaluated the relationship between *PRKAG2* methylation and the capacity for AMPK phosphorylation with 24hFA and found that *PRKAG2*: cg20534694 methylation was inversely correlated with the 24hFA-induced change in AMPK ^{Thr172}/AMPK, but only among Ob-MSCs (Figure 6D), suggesting either a threshold of methylation above which functional deficits are observed, or a combination of factors affecting AMPK function. Therefore, we next measured mRNA content of all AMPK subunit isoforms for GM and MIM conditions and observed similar patterns of deficit in Ob- versus NW-MSC for many AMPK subunits (Supplemental Figure 5). These data, combined with our initial observation of lower AMPKα1/2 protein content in all Ob-MSCs (Figure 3F) suggest that functional deficits in AMPK are likely multifactorial, including differences in DNA methylation, gene transcription, and protein activation. Moreover, ObLo and ObHi groups are likely affected differently, or to varying degrees, by variability in exposures associated with maternal obesity during intrauterine development (e.g. insulin, fatty acids, oxidative stress).

3.7. MSC DNA methylation is correlated with neonatal outcomes

Lastly, to determine how variability in maternal exposures or infant outcomes corresponds to MSC outcomes, we evaluated relationships between MSC methylation and maternal/infant *in vivo* measures. We found that *PRKAG2*:cg20534694 and *ACACB*:cg02022322 were positively correlated with cord blood insulin, while *PRKAG2*:cg20534694 was also positively correlated with infant adiposity (Supplemental Table 7, Figure 6E). Only the *PRKAG2* associations with infant fat mass or adiposity remained significant after adjusting for multiple testing.

4. DISCUSSION

Causal mechanisms of excess adiposity in infants born to mothers with obesity and the biochemical pathways contributing to the development of obesity or metabolic disease in these offspring are not clear. To begin to address this research gap, we have developed a novel model of umbilical cord-derived MSCs that may give critical insight into the mechanisms for altered metabolism in infants born to mothers with obesity. In this study, our goal was to identify potential differences in lipid metabolism in myogenic differentiating Ob-MSCs, consistent with those observed in adults with established obesity and in offspring from animal models of maternal obesity. We found that umbilical cord-derived MSCs from infants born to mothers with obesity exhibit excess lipid accumulation when undergoing myogenesis *in vitro*. Lipid accumulation was explained by lower rates of FAO and greater lipid esterification, rather than differences in lipid uptake. Our FAO assay revealed heterogeneity among Ob-MSCs, while those from infants born with highest adiposity and cord blood insulin levels consistently demonstrated lower mitochondrial FAO and AMPK activation, and greatest DNA methylation in genes encoding for proteins regulating AMPK and FAO. Moreover, despite rescue of deficits in AMPK ^{Thr172}/AMPK with 24hAICAR, these cells maintained deficits in AMPK activity. We interpret this to mean that factors associated with maternal obesity impair offspring AMPK signaling and responsiveness, resulting in

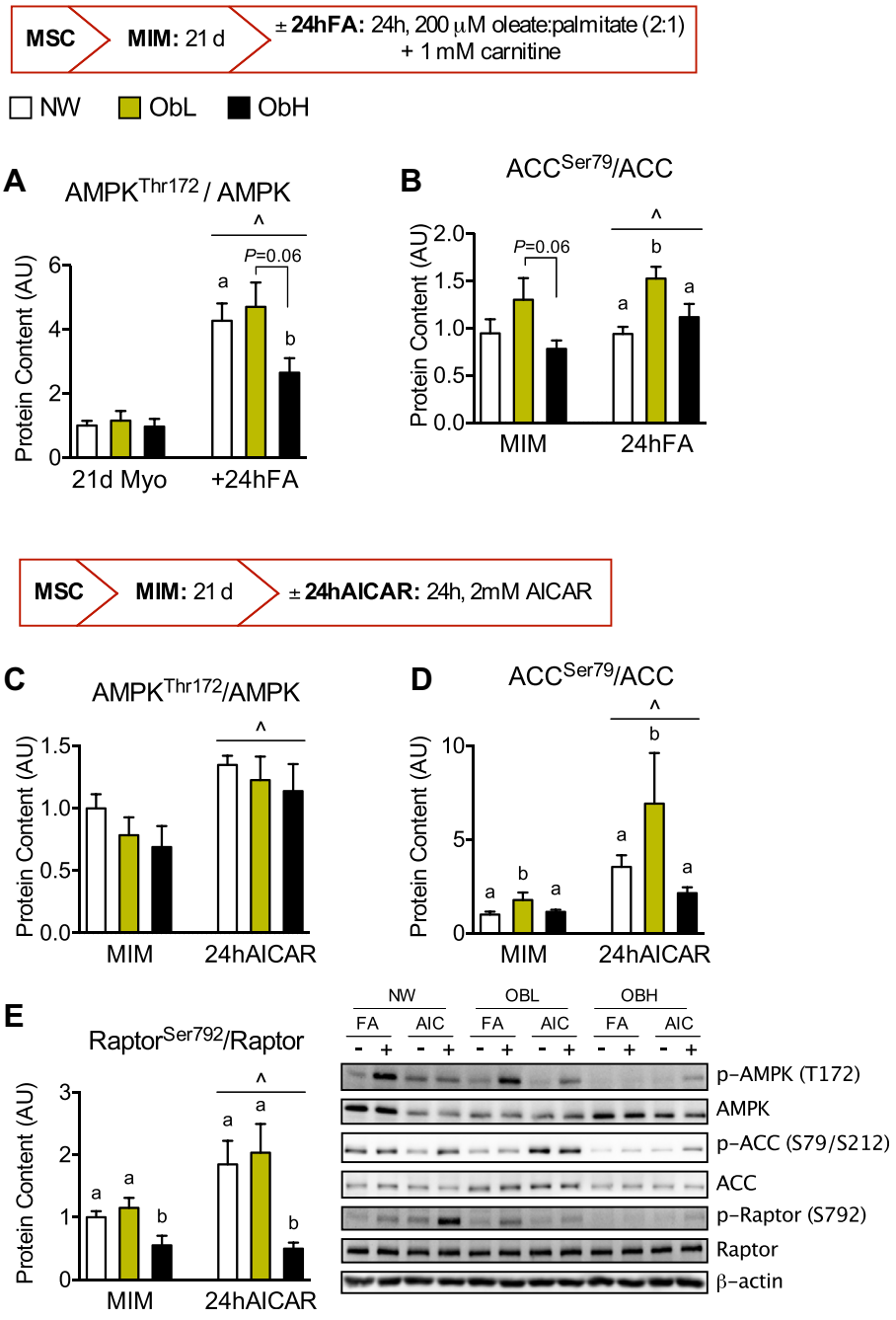

Figure 4: Lower AMPK activation in ObHi-MSCs, see also Supplemental Figure 3. At d20 of myogenesis, cells were incubated with or without excess fatty acids for 24 h in conditions depicted (24hFA), then Simple Western measures were made for (**A**) phosphorylated (Thr172) relative to total protein content of AMPKα1/α2 and (**B**) phosphorylated (Ser79) relative to total protein content of ACC. Simple Western data are presented in arbitrary units as the fold-difference in ObLo and ObHi groups relative to NW-MSCs (2 culture replicates per subject, pooled). Individual phosphorylated and total protein measures are shown in Supplemental Figure 3a–d. At d20 of myogenesis, cells were incubated with or without AICAR for 24 h in conditions depicted, followed by western blot analysis for (**C**) phosphorylated (Thr172) relative to total protein content of AMPKα1/α2, (**D**) phosphorylated (Ser79) relative to total protein content of ACC, and (**E**) phosphorylated (Ser792) relative to total protein content of Raptor. Western blot data are presented in arbitrary units as the fold-difference in ObLo and ObHi groups relative to NW-MSCs (2 culture replicates per subject, pooled). β-actin serves as a loading control. Individual phosphorylated and total protein measures are shown in Supplemental Figure 3e–j. All data are presented as mean ± SEM. For all measures n ≥ 4 subjects/group. For each panel, bars with different letters indicate differences for those groups at $P < 0.05$ as calculated by ANOVA analysis with *a priori* planned comparisons for three independent groups and comparison of NW-MSC versus all Ob-MSCs. ^ $P < 0.05$ for difference from untreated condition for both NW- and Ob-MSC groups, combined using 2-tailed paired *t*-test. MIM: myogenic induction media; AMPK, AMP-activated protein kinase; ACC, acetyl CoA carboxylase.

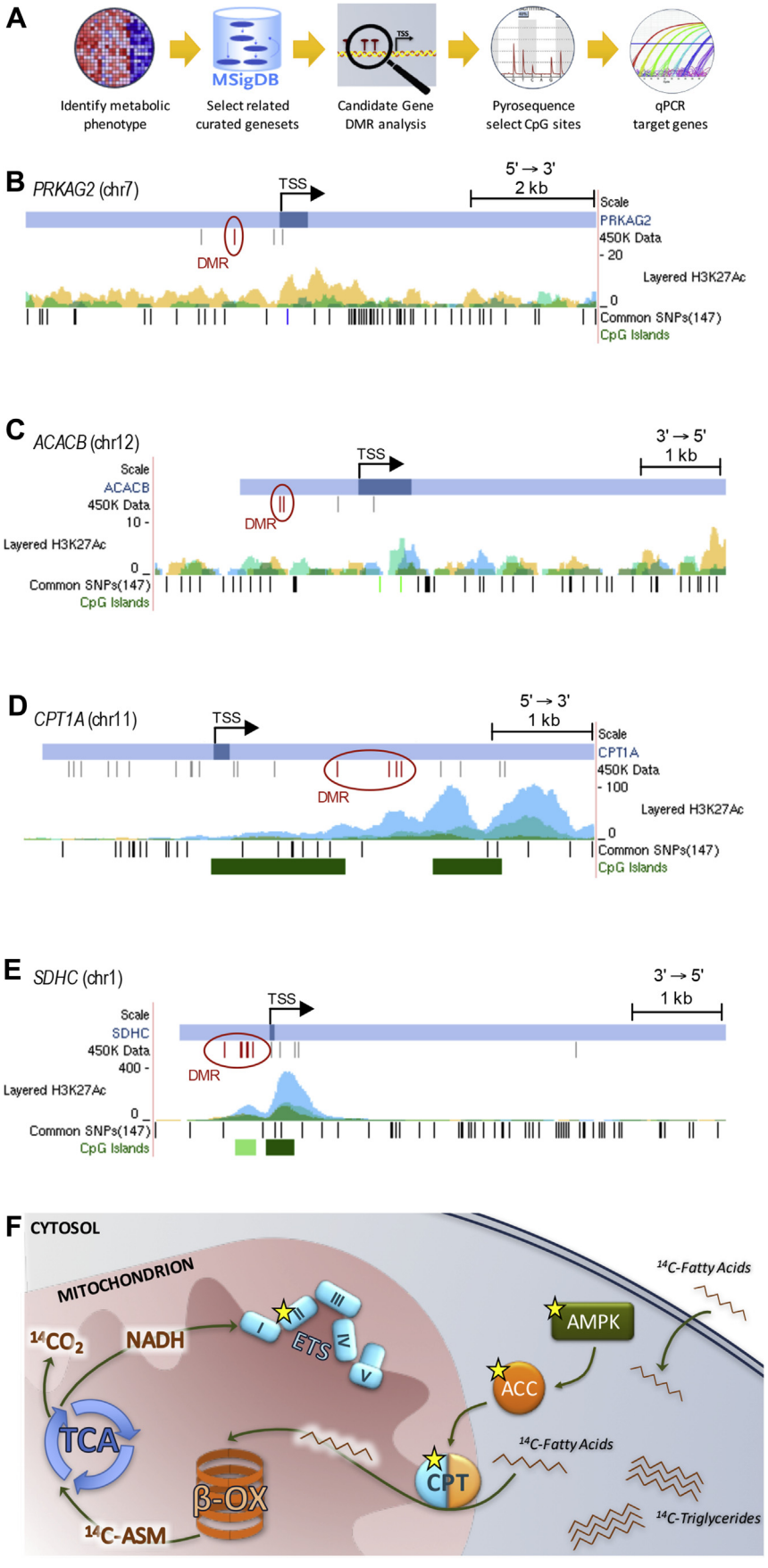

dysregulation of FAO. While the exact mechanisms underlying inter-individual susceptibility to obesity remain largely unknown, we postulate that excess infant adiposity is a strong marker of fetal exposures that underlies changes in infant stem cell DNA methylation, metabolism, and dysfunction in energy sensing pathways.

Our results are consistent with perturbations in lipid metabolism identified in skeletal muscle tissue and muscle-derived satellite cells in adults with established obesity [9,11,12] and satellite cells of offspring of obese non-human primates [10]. *In utero*, fetal MSCs differentiate into mature adipocytes and myocytes, but also maintain progenitor populations in the developed tissues (e.g., SV and satellite cells). *In vivo*, these 'adult MSCs' can differentiate to mature cells (e.g., adipocytes, myocytes) for tissue maintenance and repair. *In vitro*, these adult MSCs retain cell surface markers and differentiation capacity consistent with fetal MSCs [35]. Furthermore, adipose SV cells from adult humans born with low birth weight demonstrate reduced adipogenesis and lower leptin production *in vitro* relative to normal birthweight counterparts [36]. This was correlated with lower circulating leptin levels *in vivo* and attributed to differences in leptin gene promoter methylation *in vitro* [36]. Similarly, skeletal muscle satellite cells from adult, low birth weight cohorts also demonstrate perturbations to myogenesis and oxidative metabolism [37]. We have previously described Ob-MSC differences in adipogenesis and β-catenin signaling, similar to animal models of maternal obesity [4], and have reported Ob-MSC perturbations to metabolic and energy sensing pathways, as determined by metabolomic and RNA sequencing analyses (in press). In the aggregate, these data suggest that early perturbations in metabolism affecting the MSC lineage, and offspring mesodermal tissues, may also be observed in adult MSCs and in MSCs derived from the umbilical cord.

Disruption to AMPK proteins and gene expression are routinely observed in placenta and fetal tissues from obese dams [38–41], with some showing rescue with maternal metformin administration [41]. In humans, disruption to AMPK signaling is observed in placenta from mothers with obesity [42]. Moreover, placental tissue and isolated placental trophoblasts from mothers with obesity display reduced FAO and greater esterification that is linked to impaired mitochondrial function and perturbations to CPT1 and other FAO-related genes [43]. Though others relate these placental differences more to gestational diabetes than maternal obesity *per se* [44], overall these data suggest that a common response to maternal fuel overload, whether placenta, fetal cells, or fetal skeletal muscle tissue is reduced cellular energy sensing and increased energy storage.

We employed a hypothesis-driven approach to identify a potential epigenetic basis for the observed MSC phenotypes by limiting our methylation analysis to genesets related to oxidative metabolism. Because our goal was to first identify a metabolic phenotype based on maternal obesity exposure, our study was powered thusly. Therefore, our sample size is relatively small in comparison to epigenome-wide association studies (EWAS), but warranted for completing the in-depth metabolic phenotyping of the MSCs that is not feasible in archived tissue or blood samples. Nevertheless, our results are consistent with adult EWAS investigations, where two CpGs we identified in the *CPT1A* DMR (cg00574958 and cg17058475) were associated with blood lipid profiles in humans [45,46]. Some groups have associated differential methylation of these CpGs with intrauterine famine exposure [32,33], strengthening the hypothesis that intrauterine metabolic disturbances introduce stable epigenetic modifications in fetal cells and tissues that we are able to detect in human umbilical cord-derived MSCs. It should be noted however, that although we studied an isolated MSC population [4], MSCs are characteristically heterogeneous and differences in cell subtype may account for some portion of the differences in DNA methylation between NW- and Ob-MSCs [47,48].

Hypermethylation of genes in oxidative metabolism pathways, and corresponding down-regulation of mRNA content, suggests the MSC phenotype may be affected by multiple genes that are coordinately regulated. Thus, metabolic differences in the MSCs are likely multifactorial and may not be attributable to differences in a single CpG, or even a single DMR or gene. We have not yet determined whether these potential sites of differential methylation observed in the MSCs are causally related to mRNA differences, though this deserves further study. Since undifferentiated MSCs represent the least manipulated progenitor cell state it is less likely that our experimental procedures influenced MSC methylation. Likewise, methylation measures were made prior to excess lipid accumulation in Ob-MSCs, as there is nearly negligible lipid present in the undifferentiated cells [4]. Thus, as MSCs become committed to the myogenic lineage, emergence of the metabolic phenotype is more likely influenced by the original methylation state rather than *vice versa*. Our observation that MSC metabolic phenotype is maintained through multiple cell divisions *in vitro*, also suggests that these intrauterine exposures may have long-term consequences for offspring stem cell metabolism.

5. CONCLUSION

We have identified maternal obesity-associated reductions in offspring MSC lipid metabolism and AMPK activity. Our hypothesis that maternal obesity drives MSC phenotype was partially correct, with observed heterogeneity in Ob-MSC metabolism that corresponded to differences in infant adiposity. These distinct MSC phenotypes suggest that intrauterine exposures, rather than maternal obesity *per se*, influences MSC metabolism. While it is not possible to demonstrate that human MSC metabolism is causal to obesity risk in these children, our outcomes are consistent with metabolic phenotypes observed in offspring from animal models of maternal obesity and in adult humans with established obesity. As we continue to follow these children longitudinally, we may be better able to address whether umbilical cord MSC metabolism is predictive of future weight gain or adiposity patterns.

AUTHOR CONTRIBUTIONS

KEB conceived the MSC studies presented here. KEB and ZWP designed and carried out cell culture experiments, FAO measures,

Figure 5: Ob-MSCs exhibit DNA hypermethylation of genes specific to FAO, see also Supplemental Tables 3–5 and Supplemental Figure 4. (**A**) Graphic depicting epigenetic analysis workflow. Based on metabolic phenotype identified for FAO, we selected curated genesets specific to oxidative metabolism and employed candidate gene analysis of Illumina Infinium 450 K measures specific to these genes (see Supplemental Tables 2–3 for geneset details), four genes contained significantly differentially methylated regions (DMRs): *PRKAG2*, *ACACB*, *CPT1A* and *SDHC* (see Supplemental Table 5 and Supplemental Figure 4 for DMR/full gene details). Select CpG sites confirmed with bisulfite pyrosequencing, followed by qPCR to evaluate expression of identified genes (data shown in Figure 6). (**B**–**E**) Graphics depicting DMR loci with respect to the transcription start site (TSS); For each gene graphic, the gene is shown in blue (introns in light blue and exons in dark blue). All CpG sites measured by the 450 K are depicted with bar (450 K Data) showing. CpGs comprising significant DMRs are indicated by red circles. Location of known common SNPs, active histone methylation for similar cell types as indicated in Supplemental Figure 4, and CpG islands are shown. Full genes are shown in Supplemental Figure 4. (**F**) Graphic depicting metabolic pathways measured with location of proteins encoded by differentially methylated genes marked with stars. For all 450 K measures, n = 12 NW-MSCs and n = 12 Ob-MSC.

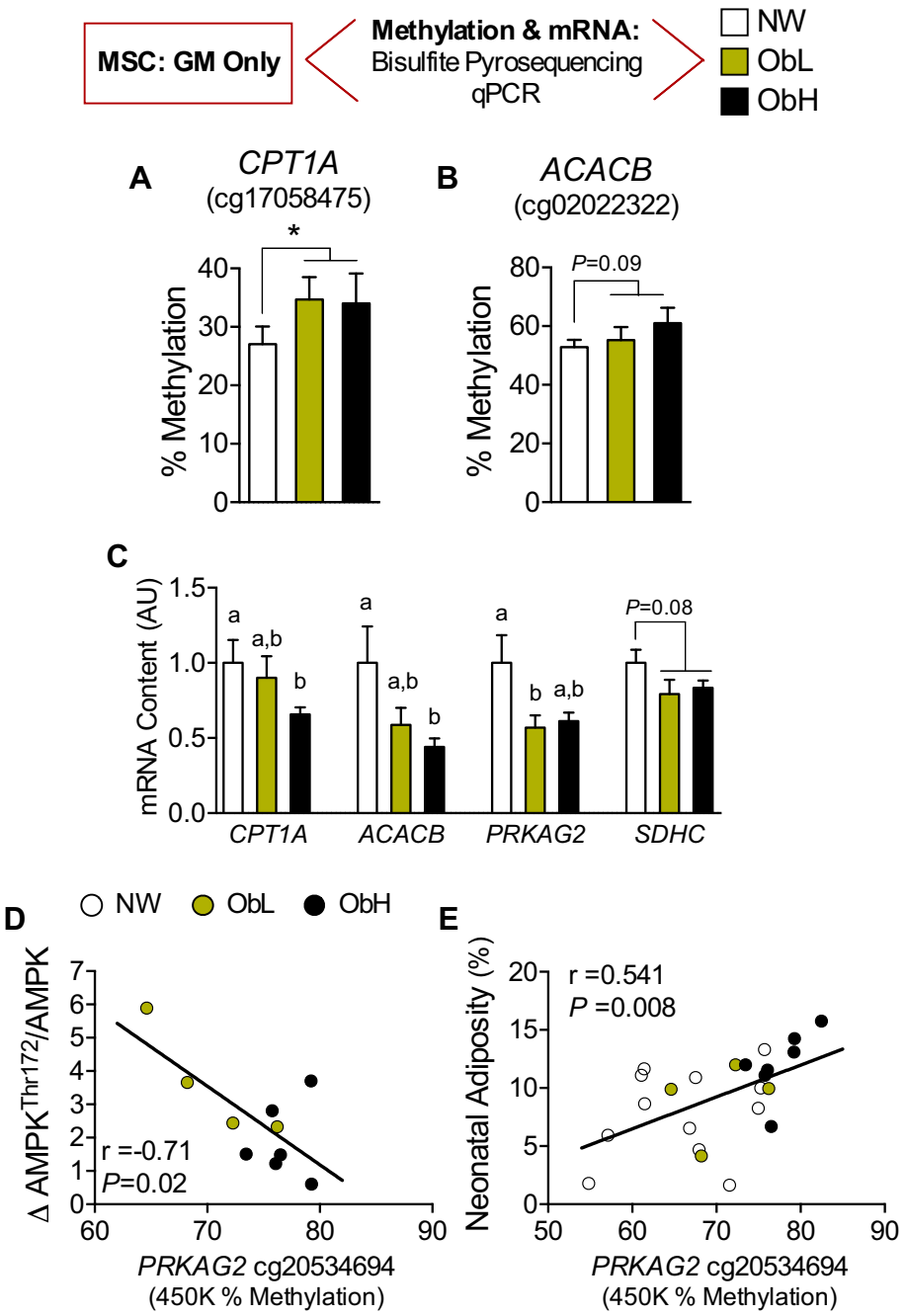

Figure 6: Ob-MSC DNA hypermethylation corresponds to lower mRNA content and is correlated with MSC and infant outcomes, see also Supplemental Figure 5, Supplemental Table 7. (**A**–**B**) Select CpG sites are shown in bar graph for bisulfite pyrosequencing measures for *CPT1A* and *ACACB*. (**C**) qPCR was used to measure mRNA content of targeted genes in the undifferentiated cells (GM; growth media). See Supplemental Figure 5 for mRNA content of all AMPK subunits. (**D**) Pearson correlation for percent methylation of *PRKAG2* cg20534694 (GM condition) and change in phospho/total AMPK protein in response to 24hFA exposure (MIM condition) was performed in the Ob-MSCs. Pearson correlation for percent methylation of *PRKAG2*:cg20534694, *ACACB*:cg02022322, *CPT1A*:17058475, and *SDHC*:08716396 *vs.* maternal fasting insulin and FFA levels, infant cord blood insulin levels, and infant body composition were performed for all subjects (Supplemental Table 7). (**D**) Significant relationship is depicted for *PRKAG2*:cg20534694 and infant adiposity. Individual data points are depicted with group coloring. For all measures, n $\geq$ 12 NW-MSCs and n $\geq$ 12 Ob-MSC. For pyrosequencing and qPCR measures there were 3 technical replicates per subject. All data are presented as mean $\pm$ SEM. For all measures n $\geq$ 4 subjects/group. For each panel, bars with different letters indicate differences for those groups at P $<$ 0.05 as calculated by ANOVA analysis with *a priori* planned comparisons for three independent groups and comparison of NW-MSC versus all Ob-MSCs.

protein and enzyme assay measures, and wrote the manuscript. CB and EJD performed pyrosequencing measures and analysis. IVY provided critical input for pyrosequencing primer design, DNA methylation analysis, and data interpretation. RJF, BKS, and GRS performed protein measures for 24hFA and AICAR experiments and provided critical input for AMPK data interpretation. LV and KK designed and performed DNA methylation analysis. KEB and JEF supervised all experiments. DD conceived, designed, and carried out the Healthy Start Study, and provided all maternal and infant clinical data. ALBS conceived, designed, and carried out the Healthy Start BabyBUMP MSC collection. All authors contributed to data analysis, interpretation, and editing of the manuscript.

ACKNOWLEDGEMENTS

This work was supported by grants from The Obesity Society (KEB), the University of Colorado Center for Women's Health Research (KEB), the Canadian Institutes of Health Research (GRS), and the Genomics and Microarray Shared Resource of Colorado's NIH/NCI Cancer Center (P30CA046934). KEB was supported by National Institutes of Health (NIH, K12HD057022 and K01DK106347). GRS is a Canada Research Chair in Metabolism and Obesity and the J. Bruce Duncan Chair in Metabolic Diseases. The Healthy Start BabyBUMP Project was supported by grants from the American Heart Association (14PRE18230008, ALBS), the Colorado Nutrition and Obesity Research Center (NORC; NIH, P30DK048520), and by the parent Healthy Start study: (NIH, R01DK076648, DD) and NIH/NCATS Colorado CTSA (UL1TR001082). Contents are the authors' sole responsibility and do not necessarily represent official views of the funding agencies.

CONFLICT OF INTEREST

None declared.

APPENDIX A. SUPPLEMENTARY DATA

Supplementary data related to this article can be found at http://dx.doi.org/10.1016/j.molmet.2017.08.012.

REFERENCES

[1] Boney, C.M., Verma, A., Tucker, R., Vohr, B.R., 2005. Metabolic syndrome in childhood: association with birth weight, maternal obesity, and gestational diabetes mellitus. Pediatrics 115(3):e290–e296. http://dx.doi.org/10.1542/peds.2004-1808.

[2] Ismail-Beigi, F., Catalano, P.M., Hanson, R.W., 2006. Metabolic programming: fetal origins of obesity and metabolic syndrome in the adult. American Journal of Physiology Endocrinology and Metabolism 291(3):E439–E440. http://dx.doi.org/10.1152/ajpendo.00105.2006.

[3] Modi, N., Murgasova, D., Ruager-Martin, R., Thomas, E.L., Hyde, M.J., Gale, C., et al., 2011. The influence of maternal body mass index on infant adiposity and hepatic lipid content. Pediatric Research 70(3):287–291. http://dx.doi.org/10.1203/PDR.0b013e318225f9b1.

[4] Boyle, K.E., Patinkin, Z.W., Shapiro, A.L.B., Baker, P.R., Dabelea, D., Friedman, J.E., 2016. Mesenchymal stem cells from infants born to obese mothers exhibit greater potential for adipogenesis: the healthy start BabyBUMP project. Diabetes 65(3):647–659. http://dx.doi.org/10.2337/db15-0849.

[5] Starling, A.P., Brinton, J.T., Glueck, D.H., Shapiro, A.L., Harrod, C.S., Lynch, A.M., et al., 2015. Associations of maternal BMI and gestational weight gain with neonatal adiposity in the healthy start study. The American Journal of Clinical Nutrition 101(2):302–309. http://dx.doi.org/10.3945/ajcn.114.094946.

[6] Brumbaugh, D.E., Tearse, P., Cree-Green, M., Fenton, L.Z., Brown, M., Scherzinger, A., et al., 2013. Intrahepatic fat is increased in the neonatal offspring of obese women with gestational diabetes. The Journal of Pediatrics 162(5):930–931. http://dx.doi.org/10.1016/j.jpeds.2012.11.017.

[7] Yan, X., Zhu, M.J., Xu, W., Tong, J.F., Ford, S.P., Nathanielsz, P.W., et al., 2010. Up-regulation of toll-like receptor 4/nuclear factor-κB signaling is associated with enhanced adipogenesis and insulin resistance in fetal skeletal muscle of obese sheep at late gestation. Endocrinology 151(1):380–387. http://dx.doi.org/10.1210/en.2009-0849.

[8] McCurdy, C.E., Bishop, J.M., Williams, S.M., Grayson, B.E., Smith, M.S., Friedman, J.E., et al., 2009. Maternal high-fat diet triggers lipotoxicity in the fetal livers of nonhuman primates. The Journal of Clinical Investigation 119(2):323–335. http://dx.doi.org/10.1172/JCI32661.

[9] Hulver, M.W., Berggren, J.R., Carper, M.J., Miyazaki, M., Ntambi, J.M., Hoffman, E.P., et al., 2005. Elevated stearoyl-CoA desaturase-1 expression in skeletal muscle contributes to abnormal fatty acid partitioning in obese humans. Cell Metabolism 2(4):251–261. http://dx.doi.org/10.1016/j.cmet.2005.09.002.

[10] McCurdy, C.E., Schenk, S., Hetrick, B., Houck, J., Drew, B.G., Kaye, S., et al., 2016. Maternal obesity reduces oxidative capacity in fetal skeletal muscle of Japanese macaques. JCI Insight 1(16):1–17. http://dx.doi.org/10.1172/jci.insight.86612.

[11] Corpeleijn, E., Saris, W.H., Blaak, E.E., 2009. Metabolic flexibility in the development of insulin resistance and type 2 diabetes: effects of lifestyle. Obesity Reviews: An Official Journal of the International Association for the Study of Obesity 10(2):178–193. http://dx.doi.org/10.1111/j.1467-789X.2008.00544.x.

[12] Ukropcova, B., McNeil, M., Sereda, O., de Jonge, L., Xie, H., Bray, G.A., et al., 2005. Dynamic changes in fat oxidation in human primary myocytes mirror metabolic characteristics of the donor. The Journal of Clinical Investigation 115(7):1934–1941. http://dx.doi.org/10.1172/JCI24332.

[13] Borengasser, S.J., Zhong, Y., Kang, P., Lindsey, F., Ronis, M.J.J., Badger, T.M., et al., 2013. Maternal obesity enhances white adipose tissue differentiation and alters genome-scale DNA methylation in male rat offspring. Endocrinology 154(11):4113–4125. http://dx.doi.org/10.1210/en.2012-2255.

[14] Yang, Q.-Y., Liang, J.-F., Rogers, C.J., Zhao, J.-X., Zhu, M.-J., Du, M., 2013. Maternal obesity induces epigenetic modifications to facilitate Zfp423 expression and enhance adipogenic differentiation in fetal mice. Diabetes 62(11):3727–3735. http://dx.doi.org/10.2337/db13-0433.

[15] Fernandez-Twinn, D.S., Alfaradhi, M.Z., Martin-Gronert, M.S., Duque-Guimaraes, D.E., Piekarz, A., Ferland-McCollough, D., et al., 2014. Down-regulation of IRS-1 in adipose tissue of offspring of obese mice is programmed cell-autonomously through post-transcriptional mechanisms. Molecular Metabolism 3(3):325–333. http://dx.doi.org/10.1016/j.molmet.2014.01.007.

[16] Godfrey, K.M., Sheppard, A., Gluckman, P.D., Lillycrop, K.A., Burdge, G.C., McLean, C., et al., 2011. Epigenetic gene promoter methylation at birth is associated with child's later adiposity. Diabetes 60(5):1528–1534. http://dx.doi.org/10.2337/db10-0979.

[17] Gang, E.J., Jeong, J.A., Hong, S.H., Hwang, S.H., Kim, S.W., Yang, I.H., et al., 2004. Skeletal myogenic differentiation of mesenchymal stem cells isolated from human umbilical cord blood. Stem Cells 22(4):617–624. http://dx.doi.org/10.1634/stemcells.22-4-617.

[18] Boyle, K.E., Friedman, J.E., Janssen, R.C., Underkofler, C., Houmard, J.A., Rasouli, N., 2017. Metabolic inflexibility with obesity and the effects of fenofibrate on skeletal muscle fatty acid oxidation. Hormone and Metabolic Research=Hormon-Und Stoffwechselforschung=Hormones et Métabolisme 49(1):50–57. http://dx.doi.org/10.1055/s-0042-111517.

[19] Kozma, L., Baltensperger, K., Klarlund, J., Porras, A., Santos, E., Czech, M.P., 1993. The ras signaling pathway mimics insulin action on glucose transporter translocation. Proceedings of the National Academy of Sciences of the United States of America 90(10):4460–4464.

[20] Boyle, K.E., Newsom, S.A., Janssen, R.C., Lappas, M., Friedman, J.E., 2013. Skeletal muscle MnSOD, mitochondrial complex II, and SIRT3 enzyme activities are decreased in maternal obesity during human pregnancy and gestational diabetes mellitus. The Journal of Clinical Endocrinology and Metabolism 98(10):E1601–E1609. http://dx.doi.org/10.1210/jc.2013-1943.

[21] Bieber, L.L., Abraham, T., Helmrath, T., 1972. A rapid spectrophotometric assay for carnitine palmitoyltransferase. Analytical Biochemistry 50(2):509–518.

[22] Smith, B.K., Ford, R.J., Desjardins, E.M., Green, A.E., Hughes, M.C., Houde, V.P., et al., 2016. Salsalate (Salicylate) uncouples mitochondria, improves glucose homeostasis, and reduces liver lipids independent of AMPK-β1. Diabetes 65(11):3352–3361. http://dx.doi.org/10.2337/db16-0564.

[23] Aryee, M.J., Jaffe, A.E., Corrada-Bravo, H., Ladd-Acosta, C., Feinberg, A.P., Hansen, K.D., et al., 2014. Minfi: a flexible and comprehensive Bioconductor package for the analysis of Infinium DNA methylation microarrays. Bioinformatics (Oxford, England) 30(10):1363–1369. http://dx.doi.org/10.1093/bioinformatics/btu049.

[24] Pidsley, R., Y Wong, C.C., Volta, M., Lunnon, K., Mill, J., Schalkwyk, L.C., 2013. A data-driven approach to preprocessing Illumina 450K methylation array data. BMC Genomics 14(1):293. http://dx.doi.org/10.1186/1471-2164-14-293.

[25] Peters, T.J., Buckley, M.J., Statham, A.L., Pidsley, R., Samaras, K., Lord, R.v., et al., 2015. De novo identification of differentially methylated regions in the human genome. Epigenetics & Chromatin 8:6. http://dx.doi.org/10.1186/1756-8935-8-6.

[26] Koves, T.R., Ussher, J.R., Noland, R.C., Slentz, D., Mosedale, M., Ilkayeva, O., et al., 2008. Mitochondrial overload and incomplete fatty acid oxidation contribute to skeletal muscle insulin resistance. Cell Metabolism 7(1):45–56. http://dx.doi.org/10.1016/j.cmet.2007.10.013.

[27] Berggren, J.R., Boyle, K.E., Chapman, W.H., Houmard, J.A., 2008. Skeletal muscle lipid oxidation and obesity: influence of weight loss and exercise. AJP: Endocrinology and Metabolism 294(4):E726–E732. http://dx.doi.org/10.1152/ajpendo.00354.2007.

[28] Consitt, L.A., Bell, J.A., Koves, T.R., Muoio, D.M., Hulver, M.W., Haynie, K.R., et al., 2010. Peroxisome proliferator-activated receptor-gamma coactivator-1alpha overexpression increases lipid oxidation in myocytes from extremely obese individuals. Diabetes 59(6):1407–1415. http://dx.doi.org/10.2337/db09-1704.

[29] Bell, J.A., Reed, M.A., Consitt, L.A., Martin, O.J., Haynie, K.R., Hulver, M.W., et al., 2010. Lipid partitioning, incomplete fatty acid oxidation, and insulin signal transduction in primary human muscle cells: effects of severe obesity, fatty acid incubation, and fatty acid translocase/CD36 overexpression. The Journal of Clinical Endocrinology and Metabolism 95(7):3400–3410. http://dx.doi.org/10.1210/jc.2009-1596.

[30] Borengasser, S.J., Faske, J., Kang, P., Blackburn, M.L., Badger, T.M., Shankar, K., 2014. In utero exposure to prepregnancy maternal obesity and postweaning high-fat diet impair regulators of mitochondrial dynamics in rat placenta and offspring. Physiological Genomics 46(23):841–850. http://dx.doi.org/10.1152/physiolgenomics.00059.2014.

[31] Fullerton, M.D., Galic, S., Marcinko, K., Sikkema, S., Pulinilkunnil, T., Chen, Z.-P., et al., 2013. Single phosphorylation sites in Acc1 and Acc2 regulate lipid homeostasis and the insulin-sensitizing effects of metformin. Nature Medicine 19(12):1649–1654. http://dx.doi.org/10.1038/nm.3372.

[32] Tobi, E.W., Goeman, J.J., Monajemi, R., Gu, H., Putter, H., Zhang, Y., et al., 2014. DNA methylation signatures link prenatal famine exposure to growth and metabolism. Nature Communications 5:5592–5614. http://dx.doi.org/10.1038/ncomms6592.

[33] Dekkers, K.F., van Iterson, M., Slieker, R.C., Moed, M.H., Bonder, M.J., van Galen, M., et al., 2016. Blood lipids influence DNA methylation in circulating cells. Genome Biology 17(1):1–12. http://dx.doi.org/10.1186/s13059-016-1000-6.

[34] Ross, F.A., Jensen, T.E., Hardie, D.G., 2016. Differential regulation by AMP and ADP of AMPK complexes containing different γ subunit isoforms. The Biochemical Journal 473(2):189–199. http://dx.doi.org/10.1042/BJ20150910.

[35] da Silva Meirelles, L., Chagastelles, P.C., Nardi, N.B., 2006. Mesenchymal stem cells reside in virtually all post-natal organs and tissues. Journal of Cell Science 119(Pt 11):2204–2213. http://dx.doi.org/10.1242/jcs.02932.

[36] Schultz, N.S., Broholm, C., Gillberg, L., Mortensen, B., Jørgensen, S.W., Schultz, H.S., et al., 2014. Impaired leptin gene expression and release in cultured preadipocytes isolated from individuals born with low birth weight. Diabetes 63(1):111–121. http://dx.doi.org/10.2337/db13-0621.

[37] Hansen, N.S., Hjort, L., Broholm, C., Gillberg, L., Schrölkamp, M., Schultz, H.S., et al., 2016. Metabolic and transcriptional changes in cultured muscle stem cells from low birth weight subjects. The Journal of Clinical Endocrinology and Metabolism 101(5):2254–2264. http://dx.doi.org/10.1210/jc.2015-4214.

[38] Rosario, F.J., Powell, T.L., Jansson, T., 2016. Activation of placental insulin and mTOR signaling in a mouse model of maternal obesity associated with fetal overgrowth. American Journal of Physiology. Regulatory, Integrative and Comparative Physiology 310(1):R87–R93. http://dx.doi.org/10.1152/ajpregu.00356.2015.

[39] Gaccioli, F., White, V., Capobianco, E., Powell, T.L., Jawerbaum, A., Jansson, T., 2013. Maternal overweight induced by a diet with high content of saturated fat activates placental mTOR and eIF2alpha signaling and increases fetal growth in rats. Biology of Reproduction 89(4):96. http://dx.doi.org/10.1095/biolreprod.113.109702.

[40] Zhu, M.J., Han, B., Tong, J., Ma, C., Kimzey, J.M., Underwood, K.R., et al., 2008. AMP-activated protein kinase signalling pathways are down regulated and skeletal muscle development impaired in fetuses of obese, over-nourished sheep. The Journal of Physiology 586(10):2651–2664. http://dx.doi.org/10.1113/jphysiol.2007.149633.

[41] Tong, J.F., Yan, X., Zhao, J.-X., Zhu, M.-J., Nathanielsz, P.W., Du, M., 2011. Metformin mitigates the impaired development of skeletal muscle in the offspring of obese mice. Nutrition & Diabetes 1(5):e7. http://dx.doi.org/10.1038/nutd.2011.3.

[42] Jansson, N., Rosario, F.J., Gaccioli, F., 2012. Activation of placental mTOR signaling and amino acid transporters in obese women giving birth to large babies. The Journal of Clinical Endocrinology & Metabolism. http://dx.doi.org/10.1210/jc.2012-2667.

[43] Calabuig-Navarro, V., Haghiac, M., Minium, J., Glazebrook, P., Ranasinghe, G.C., Hoppel, C., et al., 2017. Effect of maternal obesity on placental lipid metabolism. Endocrinology. http://dx.doi.org/10.1210/en.2017-00152.

[44] Martino, J., Sebert, S., Segura, M.T., García-Valdés, L., Florido, J., Padilla, M.C., et al., 2016. Maternal body weight and gestational diabetes differentially influence placental and pregnancy outcomes. The Journal of Clinical Endocrinology and Metabolism 101(1):59–68. http://dx.doi.org/10.1210/jc.2015-2590.

[45] Frazier-Wood, A.C., Aslibekyan, S., Absher, D.M., Hopkins, P.N., Sha, J., Tsai, M.Y., et al., 2014. Methylation at CPT1A locus is associated with lipoprotein subfraction profiles. Journal of Lipid Research 55(7):1324–1330. http://dx.doi.org/10.1194/jlr.M048504.

[46] Sayols-Baixeras, S., Irvin, M.R., Elosua, R., Arnett, D.K., Aslibekyan, S.W., 2016. Epigenetics of lipid phenotypes. Current Cardiovascular Risk Reports 10(10):31. http://dx.doi.org/10.1007/s12170-016-0513-6.

[47] Houseman, E.A., Accomando, W.P., Koestler, D.C., Christensen, B.C., Marsit, C.J., Nelson, H.H., et al., 2012. DNA methylation arrays as surrogate measures of cell mixture distribution. BMC Bioinformatics 13(1):86. http://dx.doi.org/10.1186/1471-2105-13-86.

[48] Wijetunga, N.A., Delahaye, F., Zhao, Y.M., Golden, A., Mar, J.C., Einstein, F.H., et al., 2014. The meta-epigenomic structure of purified human stem cell populations is defined at cis-regulatory sequences. Nature Communications 5:1–9. http://dx.doi.org/10.1038/ncomms6195.

